

This article was downloaded by: [Lynn M. Russell]

On: 21 January 2014, At: 09:46

Publisher: Taylor & Francis

Informa Ltd Registered in England and Wales Registered Number: 1072954 Registered office: Mortimer House, 37-41 Mortimer Street, London W1T 3JH, UK



## Aerosol Science and Technology

Publication details, including instructions for authors and subscription information:

<http://www.tandfonline.com/loi/uast20>

### Side-by-Side Comparison of Four Techniques Explains the Apparent Differences in the Organic Composition of Generated and Ambient Marine Aerosol Particles

Amanda A. Frossard<sup>a</sup>, Lynn M. Russell<sup>a</sup>, Paola Massoli<sup>b</sup>, Timothy S. Bates<sup>c</sup> & Patricia K. Quinn<sup>c</sup>

<sup>a</sup> Scripps Institution of Oceanography, UCSD, La Jolla, California, USA

<sup>b</sup> Aerodyne Research Inc., Billerica, Massachusetts, USA

<sup>c</sup> Pacific Marine Environmental Laboratory, NOAA, Seattle, Washington, USA

Published online: 21 Jan 2014.

To cite this article: Amanda A. Frossard, Lynn M. Russell, Paola Massoli, Timothy S. Bates & Patricia K. Quinn (2014) Side-by-Side Comparison of Four Techniques Explains the Apparent Differences in the Organic Composition of Generated and Ambient Marine Aerosol Particles, *Aerosol Science and Technology*, 48:3, v-x, DOI: [10.1080/02786826.2013.879979](https://doi.org/10.1080/02786826.2013.879979)

To link to this article: <http://dx.doi.org/10.1080/02786826.2013.879979>

PLEASE SCROLL DOWN FOR ARTICLE

Taylor & Francis makes every effort to ensure the accuracy of all the information (the "Content") contained in the publications on our platform. However, Taylor & Francis, our agents, and our licensors make no representations or warranties whatsoever as to the accuracy, completeness, or suitability for any purpose of the Content. Any opinions and views expressed in this publication are the opinions and views of the authors, and are not the views of or endorsed by Taylor & Francis. The accuracy of the Content should not be relied upon and should be independently verified with primary sources of information. Taylor and Francis shall not be liable for any losses, actions, claims, proceedings, demands, costs, expenses, damages, and other liabilities whatsoever or howsoever caused arising directly or indirectly in connection with, in relation to or arising out of the use of the Content.

This article may be used for research, teaching, and private study purposes. Any substantial or systematic reproduction, redistribution, reselling, loan, sub-licensing, systematic supply, or distribution in any form to anyone is expressly forbidden. Terms & Conditions of access and use can be found at <http://www.tandfonline.com/page/terms-and-conditions>



## Aerosol Research Letter

# Side-by-Side Comparison of Four Techniques Explains the Apparent Differences in the Organic Composition of Generated and Ambient Marine Aerosol Particles

Amanda A. Frossard,<sup>1</sup> Lynn M. Russell,<sup>1</sup> Paola Massoli,<sup>2</sup> Timothy S. Bates,<sup>3</sup> and Patricia K. Quinn<sup>3</sup>

<sup>1</sup>*Scripps Institution of Oceanography, UCSD, La Jolla, California, USA*

<sup>2</sup>*Aerodyne Research Inc., Billerica, Massachusetts, USA*

<sup>3</sup>*Pacific Marine Environmental Laboratory, NOAA, Seattle, Washington, USA*

## 1. INTRODUCTION

Characterizing the organic composition of marine aerosol particles is important for understanding the sources of marine aerosol and their impact on cloud microphysical properties (de Leeuw et al. 2011). A variety of measurement techniques have been used to measure the organic composition of both ambient atmospheric and freshly emitted sea spray aerosol (Table S1 in the online supplementary information [SI]). Using Fourier transform infrared (FTIR) spectroscopy, atmospheric aerosol particles collected in marine regions on multiple shipboard campaigns were shown to be saccharide-like based on their functional group composition, with a high ratio of oxygen to carbon (O/C) (Russell et al. 2010). Similarly, using scanning transmission X-ray microscopy with near-edge X-ray absorption fine structure (STXM-NEXAFS), Russell et al. (2010) and Hawkins and Russell (2010) found chemically distinct ambient marine particle types including saccharide-like components on sea salt particles and protein particles. Model ocean systems have been used to generate nascent sea spray aerosol (SSA) from seawater (Keene et al. 2007; Bates et al. 2012), to determine the organic composition of particles directly emitted from wave breaking and bubble bursting at the sea surface (Table S1). FTIR spectroscopy showed the organic composition of these generated nascent SSA, hereafter referred to as generated marine particles, also to be highly oxidized (Bates et al. 2012). In contrast, using high resolution time of flight aerosol mass spectrometry (HR-ToF-AMS) in the same study, Bates et al. (2012) found that

generated marine aerosol particles were highly unsaturated and minimally oxidized (low O/C).

In this study, we resolve this apparent discrepancy by comparing the measured organic composition of ambient and generated marine aerosol particles using these three techniques as well as a light scattering module of the HR-ToF-AMS (LS-ToF-AMS). Each of these methods is used to calculate the level of oxidation of the organic mass (OM) and assess the differences in the composition of ambient and generated marine particles. Additionally, we consider the extent to which each method provides additional insight into the particle composition.

## 2. MEASUREMENTS OF THE ORGANIC COMPOSITION OF AMBIENT AND GENERATED MARINE PARTICLES

Ambient atmospheric, which frequently included non-marine particles from the U.S east coast and shipping sources, and generated marine aerosol particles were sampled aboard the research vessel *Ronald H. Brown* during the Western Atlantic Climate Study (WACS) 19–28 August 2012. Ambient particles were sampled through two side-by-side humidity and temperature controlled masts ~18 m above sea level (Bates et al. 2002). The Sea Sweep model ocean system (Bates et al. 2012) was used to generate marine aerosol particles. Particles were characterized using four complementary techniques (Table 1): (i) FTIR spectroscopy (Russell et al. 2010); (ii) HR-ToF-AMS (DeCarlo et al. 2006); (iii) LS-ToF-AMS (Liu et al. 2013); (iv) STXM-NEXAFS (Hawkins and Russell 2010). The SI has details for particle collection and OM analysis, as well as organic carbon (OC) measurements by evolved gas analysis (EGA) of quartz filters. The range of particle aerodynamic diameters ( $d_a$ ) measured by each method is shown in Table 1 and Figure S1.

Received 20 September 2013; accepted 26 December 2013.

Address correspondence to Lynn M. Russell, Scripps Institution of Oceanography, UCSD, La Jolla, CA 92037, USA. E-mail: lmrussell@ucsd.edu

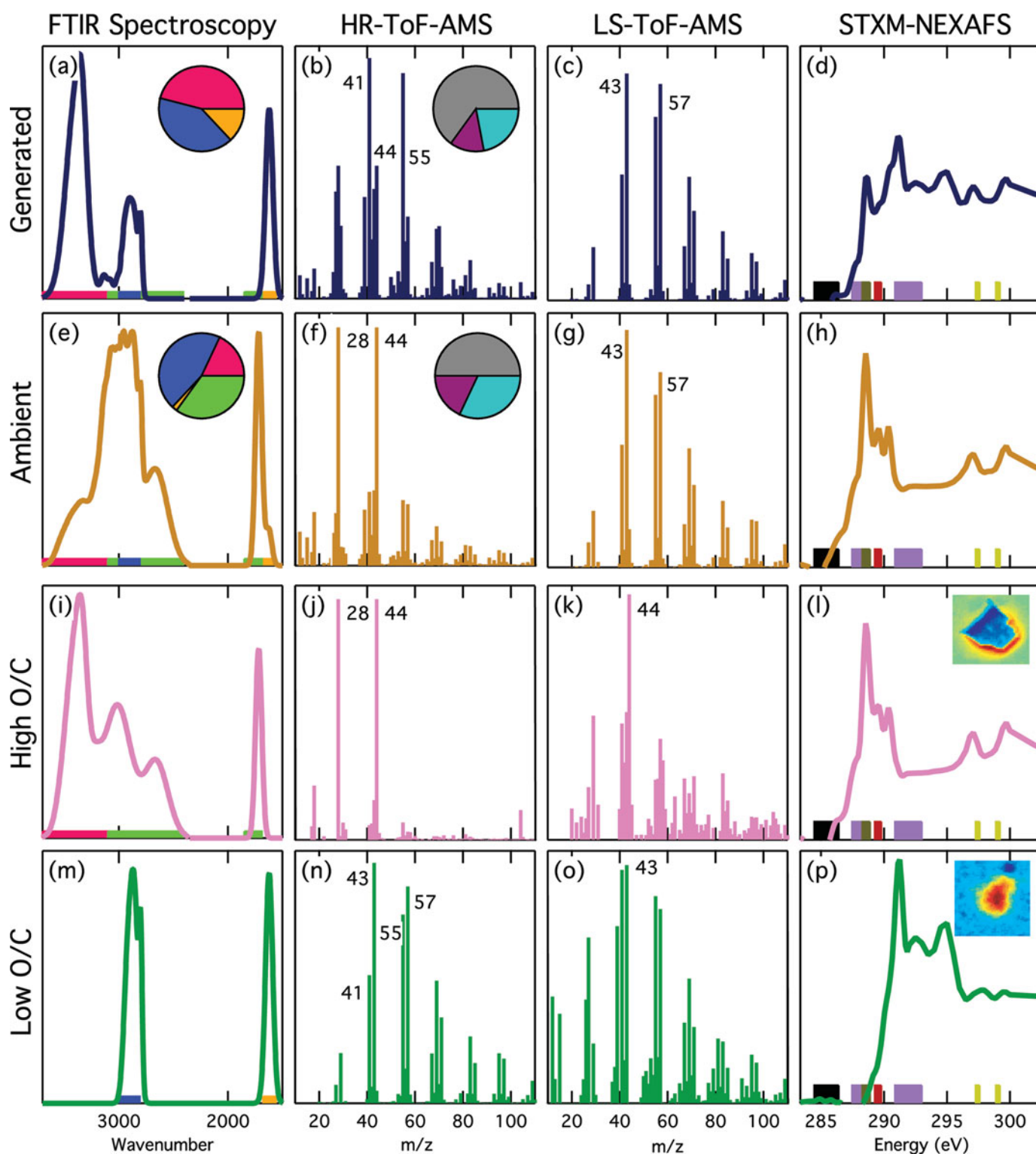


FIG. 1. Normalized spectra of (a–d) generated and (e–h) ambient marine OM and (i–l) high O/C and (m–p) low O/C particle OM types, colored across the rows as dark blue, bronze, light pink, and dark green, respectively. Columns represent the four measurement techniques. FTIR spectroscopy pies show the average functional group composition including: carboxylic acid (lime green), hydroxyl (bright pink), amine (orange), and alkane (blue). The color bars show the functional group absorption regions, using the same colors. HR-ToF-AMS pies show the average OM mass fragment group composition with  $C_xH_yO_{>1}$  (gray),  $C_xH_yO_1$  (dark purple), and  $C_xH_y$  (teal). Specific m/z values are labeled in the HR-ToF-AMS and LS-ToF-AMS panels. In the STXM-NEXAFS panel, density maps (inset in l and p) illustrate the typical particle morphology and are colored as low (blue) to high (red) probability of carbon. Color bars (left to right) represent aromatic (black), alkyl (purple), carboxylic carbonyl (brown), and alcohol (red) functional group and potassium (yellow) absorption regions for the STXM-NEXAFS spectra.

TABLE 1

Descriptions of the four techniques used to measure marine organic composition and the separation of the low and high O/C OM

Technique	Resolution (Samples)	Particle Size Range <sup>a</sup>			Low O/C <sup>b</sup>	High O/C <sup>b</sup>
		d <sub>a</sub>	d <sub>p</sub> (ρ = 1.1 g cm <sup>-3</sup> )	d <sub>p</sub> (ρ = 2.05 g cm <sup>-3</sup> )		
FTIR Spectroscopy	Bulk filter samples; 1–8 h (5 ambient, 16 Sea Sweep)	<750 nm (<1 μm) <sup>c</sup>	<682 nm (<909 nm) <sup>c</sup>	<366 nm (<488 nm) <sup>c</sup>	Alkane and amine functional groups	Hydroxyl and carboxylic acid functional groups
HR-ToF-AMS	2 min (continuous)	90–700 nm (<1 μm) <sup>d</sup>	82–636 nm (< 909 nm) <sup>d</sup>	44–341 nm (<488 nm) <sup>d</sup>	Mass fragment group C <sub>x</sub> H <sub>y</sub>	Mass fragment groups C <sub>x</sub> H <sub>y</sub> O and C <sub>x</sub> H <sub>y</sub> O <sub>&gt;1</sub>
LS-ToF-AMS	Single particles (384 ambient, 7319 generated)	180–700 nm (430 nm – 1 μm) <sup>e</sup>	164–636 nm (391–909 nm) <sup>e</sup>	88–341 nm (210–488 nm) <sup>e</sup>	Particles with CH mass fragment signature, m/z 41, 43, 55, 57	Particles with high m/z 44 mass fragments
STXM-NEXAFS	Single particles (18 ambient, 26 generated)	0.39–3.1 μm <sup>f</sup>	0.39–3.1 μm <sup>f</sup>		Particles spectra with alkyl and aromatic functional groups	Particle spectra with carboxylic carbonyl and alcohol functional groups

<sup>a</sup>Aerodynamic diameter (d<sub>a</sub>) and physical diameter (d<sub>p</sub>) particles sizes that have 100% transmission efficiency to the detector (HR-ToF-AMS and LS-ToF-AMS) and filters, with 50% transmission efficiency in parentheses. Physical diameters for FTIR, HR-ToF-AMS, and LS-ToF-AMS were calculated using densities of 1.1 and 2.05 g cm<sup>-3</sup> to represent purely organic particles and particles with 11% organics and 89% sea salt, respectively.

<sup>b</sup>Low O/C OM also contains functional groups and fragment groups with calculated O/C values of 0. High O/C OM contains any oxidized OM.

<sup>c</sup>Gussman et al. (2002); particles less than 100 nm are not collected as efficiently.

<sup>d</sup>DeCarlo et al. (2006); Jayne et al. (2000); Williams et al. (2013); 30% transmission efficiency at 1 μm.

<sup>e</sup>Liu et al. (2013); Williams et al. (2013); 180 nm are the smallest particles that produce significant optical signals; 30% transmission efficiency at 1 μm.

<sup>f</sup>Diameter range of measured particles (physical). Aerodynamic diameters were calculated from physical diameters for individual particles.

Based on FTIR spectroscopy, the OM in generated marine particles contained on average 46% hydroxyl, 41% alkane, and 13% amine functional groups (Figure 1a). The average composition of the ambient OM was 18% hydroxyl, 45% alkane, 2% amine, and 35% carboxylic acid functional groups (Figure 1e). This corresponds to average O/C values of  $0.55 \pm 0.17$  and  $0.51 \pm 0.22$  for ambient and generated marine particles, respectively (Table S3). Carboxylic acid and hydroxyl functional groups have high O/C ratios, while alkane and amine functional groups contain no oxygen (O/C = 0) and are grouped here as low O/C (Table 1; Figure 1i and 1m). Using this distinction, the generated OM was 46% high O/C and 54% low O/C organic components ( $\pm 12\%$ ), while the ambient OM was 53% and 47%  $\pm 10\%$ , respectively (Figure 2). This composition is similar to previous FTIR spectroscopy measurements of generated marine OM with 53% high O/C and 47% low O/C (Bates et al. 2012) and ambient marine OM with 55% high O/C and 45% low O/C (including 4% organosulfate functional groups) (Hawkins et al. 2010).

The organic composition measured by the HR-ToF-AMS was split into ion families based on high-resolution data analysis (SI). The first group is C<sub>x</sub>H<sub>y</sub>, which has the characteristic ion pattern from the alkane series C<sub>x</sub>H<sub>2y-1</sub><sup>+</sup> and C<sub>x</sub>H<sub>2y+1</sub><sup>+</sup>, with C<sub>3</sub>H<sub>5</sub><sup>+</sup> (m/z = 41), C<sub>3</sub>H<sub>7</sub><sup>+</sup> (m/z = 43), C<sub>4</sub>H<sub>7</sub><sup>+</sup> (m/z = 55) and C<sub>4</sub>H<sub>9</sub><sup>+</sup> (m/z = 57) among the main peaks. The second group is represented by C<sub>x</sub>H<sub>y</sub>O<sub>1</sub><sup>+</sup>, which is slightly oxidized and typically contains C<sub>2</sub>H<sub>3</sub>O<sup>+</sup> (m/z = 43) and CHO<sup>+</sup> (m/z = 29). The third group is C<sub>x</sub>H<sub>y</sub>O<sub>>1</sub><sup>+</sup>, which contains the most oxidized ions and has the highest content of CO<sub>2</sub><sup>+</sup> (m/z = 44).

The generated and ambient marine OM compositions were 22% C<sub>x</sub>H<sub>y</sub>O<sub>>1</sub>, 13% C<sub>x</sub>H<sub>y</sub>O<sub>1</sub>, and 65% C<sub>x</sub>H<sub>y</sub> and 32% C<sub>x</sub>H<sub>y</sub>O<sub>>1</sub>, 18% C<sub>x</sub>H<sub>y</sub>O<sub>1</sub>, and 50% C<sub>x</sub>H<sub>y</sub>, respectively (Figures 1b and 1f). This composition is consistent with previous HR-ToF-AMS results from similar measurements (Bates et al. 2012). Other organic fragment groups, including C<sub>x</sub>H<sub>y</sub>O<sub>>1</sub>N, C<sub>x</sub>H<sub>y</sub>O<sub>1</sub>N, and C<sub>x</sub>H<sub>y</sub>N, contribute less than 2% to the total OM and are excluded from this analysis. When grouping C<sub>x</sub>H<sub>y</sub>O<sub>1</sub> and C<sub>x</sub>H<sub>y</sub>O<sub>>1</sub> as high O/C and C<sub>x</sub>H<sub>y</sub> as low O/C (Figure 1j and

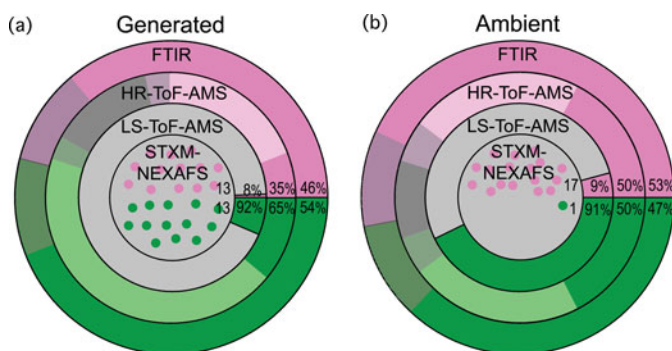


FIG. 2. Comparison of the OM composition for the (a) generated marine and (b) ambient atmospheric marine particles. The OM is separated into high O/C (pink) and low O/C (green). Gray shading in the FTIR pies represents uncertainty (see the SI). For the HR-ToF-AMS pies, the lighter shading shows the  $CE_{IC}$  that was applied, gray shading is the uncertainty (see the SI), and the dark gray is the percent difference between the FTIR and HR-ToF-AMS OM. In the LS-ToF-AMS pies, the light gray area is the number based  $CE_{LS}$ . The individual circles that make up the STXM-NEXAFS pies represent the small number of particles measured by the technique, and the numbers of particles are written in each section of the pie. The light gray shading represents the overall lower particle statistics and higher uncertainty for the STXM-NEXAFS measurements. For the HR-ToF-AMS and FTIR spectroscopy pies, the percent of the total OM that is high and low O/C are included, and for the LS-ToF-AMS, the percent of total organic particles that are high and low O/C are included.

In), the composition of the generated OM is 35% high O/C and 65% low O/C, while the ambient OM is 50% high O/C and 50% low O/C (Figure 2). This corresponds to average O/C values of  $0.63 \pm 0.11$  for ambient aerosol particles and  $0.20 \pm 0.08$  for generated marine particles, respectively (Table S3).

The HR-ToF-AMS collection efficiency (which includes lens transmission efficiency, detector efficiency, and losses due to particle bounce) was calculated by comparing HR-ToF-AMS sulfate to IC sulfate ( $CE_{IC}$ , see the SI). The ambient  $CE_{IC}$  is 0.35, and the generated  $CE_{IC}$  is 0.17 (lighter shading in Figure 2). After the  $CE_{IC}$  was applied to the HR-ToF-AMS measurements, the FTIR OM and HR-ToF-AMS OM agreed within the instrument uncertainties with an overall average percent difference of 12%. Correlations are shown in Figure S2. Because the  $CE_{IC}$  may be size-dependent, the composition of the unmeasured OM may not be the same as the measured OM. Comparisons of the FTIR and HR-ToF-AMS OM with EGA OC are shown in the SI. The HR-ToF-AMS measurements were also used to calculate the mass of sea salt and the  $CE_{total}$ , which includes sea salt ( $CE_{SS}$ ), described in the SI.

The LS-ToF-AMS optically detected 7,300 generated and 360 ambient single particles, and their average spectra are shown in Figure 1c and 1g, respectively. Of the ambient single particles that were optically detected, 47% of the particles had corresponding mass spectra that had total signal to noise (S/N) exceeding 3 (LS+MS) (SI). This result is consistent with previously measured LS+MS fractions of 0.52 (Liu et al. 2013). This corresponds to a total ambient LS-ToF-AMS CE ( $CE_{LSA}$ )

of 0.47 (gray area of Figure 2b), which is consistent with the HR-ToF-AMS  $CE_{totalA}$  of 0.49 (which includes sea salt, see the SI). For the generated particle sampling, only 7% of the particles had corresponding mass spectra with total S/N exceeding 3 (LS+MS), which corresponds to a generated marine  $CE_{LSG}$  of 0.07 (gray area of Figure 2b) and is consistent with  $CE_{totalG}$  of 0.07 (SI).

The LS+MS particle mass spectra were clustered based on their organic signal using the method outlined by Liu et al. (2013). To identify organic types, only signals at selected organic  $m/z$  values were used ( $m/z$  20, 22, 24–27, 29, 31, 40–45, 47, 49–59, 61–63, 65–79, 82–90, 92–97, 98–110). Particles with spectra that contained less than six organic ions ( $\sim 50\%$  of the LS+MS particles) were not included in the clustering. The cluster analysis separated the particles with  $C_XH_Y$  hydrocarbon-like signatures (low O/C), including  $m/z$  41, 43, 55, 57 (Figure 1o), from those with  $m/z$  44 (high O/C, due to the oxidized  $CO_2^+$  fragment) (Figure 1k). The organic fraction of ambient particles is 9% high O/C and 91% low O/C, while the generated particles is 8% high O/C and 92% low O/C (Figure 2).

The average STXM-NEXAFS spectra of the generated and ambient marine particles are shown in Figure 1d and 1h, respectively. The particle spectra were grouped using Ward cluster analysis, resulting in two types: high O/C and low O/C organics, based on functional group peaks. The high O/C group (Figure 1i) contains particle spectra with high absorbance in the carboxylic carbonyl region (288.2–288.9 eV) and varying absorption in the alcohol region (289.5 eV), which are both oxidized and considered high O/C. The second type of particle spectra, low O/C group (Figure 1p), did not contain oxidized functional groups but instead showed absorbance only in the two alkyl regions (287.4–288.5 eV for C-H bonds and 290.8–293 eV for C-C bonds). One spectrum in this type also had absorbance from 284.4–286.4 eV, indicative of aromatic or alkene functional groups. Of the 26 generated particles, 13 had high O/C spectra. For the ambient particles, 17 of 18 particles had high O/C spectra (Figure 2). The particle morphologies provided by STXM-NEXAFS are discussed in the SI. All of the generated high O/C particles were identified as similar to saccharides on sea salt, indicating that high O/C OM in the generated particles is associated with sea salt.

### 3. COMPARISON OF MEASUREMENT TECHNIQUES

The OM composition of ambient atmospheric and generated marine aerosol was measured by four complementary techniques and classified into two types of OM: high O/C OM which is highly oxidized and low O/C OM which has little or no oxidation. For the four techniques, OM was separated by: (i) functional groups with high and low O/C (FTIR spectroscopy), (ii) mass fragments with  $C_XH_YO_{>1}$ ,  $C_XH_YO_1$ , and  $C_XH_Y$  (HR-ToF-AMS), (iii) single particles with high  $m/z$  44 or  $C_XH_Y$  signatures (LS-ToF-AMS), and (iv) single particles that were alkyl-like or oxidized (STXM-NEXAFS). The high and

low O/C classification of OM provides a basis to compare the four measurement techniques (Figure 2). While the techniques have different capabilities for sampling the high and low O/C OM compositions, the composition of the particles measured by HR-ToF-AMS and FTIR spectroscopy are generally consistent. The larger differences in the generated marine particle composition can be explained by the influence of the high fraction of larger diameter sea salt containing particles that were missed by the AMS techniques and by the uncertainties of both the FTIR and AMS techniques.

STXM-NEXAFS measurements provide examples of single-particle morphology for two generated marine particle types: high O/C OM on sea salt particles (similar to particles identified previously as saccharides on sea salt (Hawkins and Russell 2010)) and low O/C OM particles (Figure 1l and 1p). Of the ambient particles, 13 of 17 of the high O/C particles were also similar to saccharides on sea salt (Figure 1l). This morphology of a small fraction of saccharide-like organic components compared to sea salt (for particles with  $d_a$  of 0.47 to 6.4  $\mu\text{m}$  that the STXM-NEXAFS sees) results in particles that are largely refractory at 650°C and, hence, may bounce off the vaporizer. The alkyl-like (low O/C OM) particle type has a more uniform morphology with OM throughout the particle and no evidence of sea salt (Figure 1p), consistent with these particles being vaporized more efficiently at 650°C than the high O/C OM on sea salt. The less than 100 particles analyzed with this technique were selected manually based on the carbon content detected and do not represent the entire OM particle population. However, the identification of both high and low O/C particle types provides consistency with the FTIR and AMS techniques, in addition to showing that the high O/C OM is typically present on the sea-salt-containing particles, especially in the generated marine aerosol.

The HR-ToF-AMS and FTIR measured compositions are similar for ambient particles both with approximately 50% high O/C OM, but there is a larger difference in the generated OM with a HR-ToF-AMS high O/C fraction of 35% and an FTIR high O/C fraction of 46% (Figure 2). This larger difference is due to the high (89%) sea salt fraction of these particles (SI). The HR-ToF-AMS measures nonrefractory particles only and is influenced by particle bounce effects. Even at 650°C, sea salt is inefficiently vaporized in the AMS. Any OM present on sea salt particles, as observed in the STXM-NEXAFS morphology, is also inefficiently vaporized in the HR-ToF-AMS. The larger fraction of low O/C OM measured by HR-ToF-AMS, compared to FTIR is a result of the high O/C OM that is associated with sea salt and low transmission efficiency of the larger sea salt particles.

The OM composition as determined by FTIR spectroscopy and HR-ToF-AMS are more similar for the ambient particles (within 10%, Figure 2b), due to the smaller fraction of sea salt in the ambient particles. If all of the sea salt (3% of the particle mass) is from sea spray and has the same ratio of OM to sea salt as the generated particles (11:89, Table S2), only 0.37% of

the particle mass is associated with sea salt, which is less than 1% of the total OM. The OM that is not associated with sea salt is nonrefractory and less influenced by bounce effects and is sampled efficiently by both the FTIR and CE-corrected AMS techniques.

The LS-ToF-AMS measurements demonstrate that a large number (93%) of generated marine particles are not vaporized in the AMS and are refractory or bounce off the vaporizer, even though they are optically detected by light scattering. The large fraction of LS-only particles observed during sampling generated marine particles is consistent with a large fraction of sea salt in those particles, compared to the lower fraction of sea salt in the ambient particles. The submicron generated particles were 89% sea salt (Table S2), consistent with an LS-only fraction of 93%. Additionally, the ratio of LS+MS particles to total particles observed by light scattering is negatively correlated with sea-salt concentrations ( $r = -0.60$ ). This result implies that the sea-salt particles detected by LS are not vaporized (no mass spectrum with total S/N exceeding 3 is obtained), consistent with the refractory nature of sea salt (which contributes to particle bounce) and the morphology measured by STXM-NEXAFS.

The composition of the LS-ToF-AMS particles includes a much higher low O/C fraction than the other techniques, for both generated and ambient particles (Figure 2). This is the result of a disproportionately low representation of the high O/C OM associated with refractory sea salt. Additionally, the LS-ToF-AMS measures single particles in a limited size range, which may not be directly comparable to the other techniques that include larger (STXM-NEXAFS and FTIR) and smaller (HR-ToF-AMS) particles (Table 1 and Figure S1). See the SI for more discussion.

#### 4. IMPLICATIONS FOR MARINE ORGANIC AEROSOL COMPOSITION

The results of the HR-ToF-AMS and FTIR measurement techniques show consistent OM concentrations and comparable high and low O/C fractions for ambient atmospheric aerosol. The discrepancy in the results was greater for the generated OM, consistent with the larger fraction of refractory particles. The sea-salt particles and associated OM do not vaporize at 650°C and are more prone to particle bounce. For both aerosol types, the high O/C OM consists of hydroxyl and carboxylic acid functional groups measured by FTIR spectroscopy and STXM-NEXAFS and mass fragments of the  $\text{C}_x\text{H}_y\text{O}_1$  and  $\text{C}_x\text{H}_y\text{O}_{>1}$  groups measured by LS-ToF-AMS and HR-ToF-AMS. The low O/C OM consists of alkane and alkyl functional groups measured by FTIR spectroscopy and STXM-NEXAFS and  $\text{C}_x\text{H}_y$  mass fragments measured by LS-ToF-AMS and HR-ToF-AMS.

The FTIR spectroscopy and HR-ToF-AMS high and low O/C fractional composition show good agreement for the ambient marine measurements, with O/C approximately 50% of the total OM. The generated marine OM fractions measured by the

HR-ToF-AMS and FTIR spectroscopy have differences up to 31%. This is consistent with the larger fraction of sea-salt particles in the generated marine OM, compared to the ambient marine OM and the larger fraction of high O/C OM associated with the sea-salt particles. With the  $CE_{IC}$  correction applied, the average ratio of HR-ToF-AMS to FTIR spectroscopy OM is 0.86, which is within the 20% uncertainty for these measurements.

STXM-NEXAFS measurements show both high O/C and low O/C particles are present in the generated marine OM, which is similar to the FTIR spectroscopy and HR-ToF-AMS measured compositions. The difference in the generated and ambient marine particle composition compared to FTIR spectroscopy and HR-ToF-AMS is likely the result of the low counting statistics and the selection of particles for analysis. The LS-ToF-AMS measurements demonstrate that a large number of the optically detected marine generated particles are not vaporized in the AMS. The result is a disproportionately high representation of the low O/C particles in the mass spectra for the LS-ToF-AMS (SI).

#### ACKNOWLEDGMENTS

The authors gratefully acknowledge Leah Williams, William Brooks, Timothy Onasch, Donna Sueper, and Shang Liu for their assistance in preparing the HR-ToF-AMS and LS-ToF-AMS for deployment and for guidance with the LS-ToF-AMS analysis. They thank the captain, crew, and scientists aboard the *Ronald H. Brown* for their support. The authors thank Derek Coffman, Drew Hamilton, and Janin Guzman-Morales for assistance with sample collection. They acknowledge David Kilcoyne at the Lawrence Berkeley National Laboratory Advanced Light Source and Satoshi Takahama for assistance with STXM-NEXAFS and beamline operation.

#### SUPPLEMENTAL MATERIAL

Supplemental data for this article can be accessed on the publisher's website.

#### REFERENCES

- Bates, T. S., et al. (2012). Measurements of Ocean Derived Aerosol off the Coast of California. *J. Geophys. Res.-Atmos.*, 117(D00V15), doi:10.1029/2012JD017588.
- Bates, T. S., Coffman, D. J., Covert, D. S., and Quinn, P. K. (2002). Regional Marine Boundary Layer Aerosol Size Distributions in the Indian, Atlantic, and Pacific Oceans: A Comparison of INDOEX Measurements With ACE-1, ACE-2, and Aerosols99. *J. Geophys. Res.-Atmos.*, 107(D19), doi:10.1029/2001jd001174.
- DeCarlo, P. F., et al. (2006). Field-Deployable, High-Resolution, Time-of-Flight Aerosol Mass Spectrometer. *Anal. Chem.*, 78(24):8281–8289, doi:10.1021/ac061249n.
- de Leeuw, G., Andreas, E. L., Anguelova, M. D., Fairall, C. W., Lewis, E. R., O'Dowd, C., et al. (2011). Production Flux of Sea Spray Aerosol. *Rev. Geophys.*, 49, doi:10.1029/2010rg000349.
- Gussman, R. A., Kenny, L. C., Labickas, M., and Norton, P. (2002). Design, Calibration, and Field Test of a Cyclone for PM1 Ambient Air Sampling. *Aerosol Sci. Technol.*, 36(3):361–365, doi:10.1080/027868202753504461.
- Hawkins, L. N., and Russell, L. M. (2010). Polysaccharides, Proteins, and Phytoplankton Fragments: Four Chemically Distinct Types of Marine Primary Organic Aerosol Classified by Single Particle Spectromicroscopy. *Adv. Meteorol.*, (Article ID 612132), 14, doi:10.1155/2010/612132.
- Hawkins, L. N., Russell, L. M., Covert, D. S., Quinn, P. K., and Bates, T. S. (2010). Carboxylic Acids, Sulfates, and Organosulfates in Processed Continental Organic Aerosol Over the Southeast Pacific Ocean During VOCALS-REx 2008. *J. Geophys. Res.-Atmos.*, 115(D13201), doi:10.1029/2009jd013276.
- Jayne, J. T., Leard, D. C., Zhang, X. F., Davidovits, P., Smith, K. A., Kolb, C. E., and Worsnop, D. R. (2000). Development of an Aerosol Mass Spectrometer for Size and Composition Analysis of Submicron Particles. *Aerosol Sci. Technol.*, 33(1–2):49–70.
- Keene, W. C., et al. (2007). Chemical and Physical Characteristics of Nascent Aerosols Produced by Bursting Bubbles at a Model Air-Sea Interface. *J. Geophys. Res.-Atmos.*, 112(D21202), doi:10.1029/2007jd008464.
- Liu, S., Russell, L. M., Sueper, D. T., and Onasch, T. B. (2013). Organic Particle Types by Single-Particle Measurements Using a Time-of-Flight Aerosol Mass Spectrometer Coupled With a Light Scattering Module. *Atmos. Meas. Tech.*, 6(2), 187–197, doi:10.5194/amt-6-187-2013.
- Russell, L. M., Hawkins, L. N., Frossard, A. A., Quinn, P. K., and Bates, T. S. (2010). Carbohydrate-Like Composition of Submicron Atmospheric Particles and Their Production From Ocean Bubble Bursting. *Proc. Natl. Acad. Sci. USA*, 107(15):6652–6657, doi:10.1073/pnas.0908905107.
- Williams, L. R., et al. (2013). Characterization of an Aerodynamic Lens for Transmitting Particles Greater Than 1 Micrometer in Diameter Into the Aerodyne Aerosol Mass Spectrometer. *Atmos. Meas. Tech.*, 6:3271–3280, doi:10.5194/amt-6-3271-2013.

## Supplemental Information

### Side-by-Side Comparison of Four Techniques Explains the Apparent Differences in the Organic Composition of Generated and Ambient Marine Aerosol Particles

Amanda A. Frossard<sup>a</sup>, Lynn M. Russell<sup>a</sup>, Paola Massoli<sup>b</sup>, Timothy S. Bates<sup>c</sup>, and Patricia K. Quinn<sup>c</sup>

<sup>a</sup>*Scripps Institution of Oceanography, UCSD, La Jolla, CA 92037*

<sup>b</sup>*Aerodyne Research Inc., Billerica, MA 01821*

<sup>c</sup>*Pacific Marine Environmental Laboratory, NOAA, Seattle, WA 98115*

#### Marine OM Measurement Techniques

The composition of the organic component of both ambient and generated marine aerosol particles differ substantially in recently reported results (Rinaldi et al. 2010; Bates et al. 2012). The cause of the difference, attributed to either different OM measurement approaches or differences in seawater properties that produce the marine particles, is still unresolved (Rinaldi et al. 2010). The purpose of this study is to resolve the discrepancy in OM composition of generated marine aerosol as observed by Fourier transform infrared (FTIR) spectroscopy and high resolution time of flight aerosol mass spectrometry (HR-ToF-AMS) measurements through the use of multiple measurement techniques including FTIR spectroscopy, HR-ToF-AMS, evolved gas analysis (EGA), scanning transmission X-ray microscopy near edge absorption fine structure (STXM-NEXAFS), and a light scattering module of the HR-ToF-AMS (LS-ToF-AMS).

Given the complexity of the organic composition of marine aerosol particles, characteristics can be determined through the combination of techniques that provide complementary information. The measurement techniques vary in the fraction of OM they can quantify and in the degree to which the organics can be speciated. Spectroscopy techniques (FTIR, Raman, and nuclear magnetic resonance) can be used to determine the functional group composition, while mass spectrometry techniques (gas chromatography mass spectrometry and aerosol mass spectrometry) can be used to determine mass fragments. These techniques and others have been utilized to measure the organic composition of ambient and generated marine aerosol particles. The multiple techniques used and the general organic compositions of marine aerosol determined by each are shown in Table S1.

Table S1: Organic composition of generated and ambient marine aerosol particles measured using different techniques.

<b>Technique Used<sup>a</sup></b>	<b>OM Composition</b>	<b>Reference</b>
<b>Ambient</b>		
FT-ICR MS; H-NMR	Biomolecules with high aliphaticity	(Schmitt-Kopplin et al. 2012)
FTIR spectroscopy and STXM-NEXAFS	Polysaccharides	(Russell et al. 2010)
GC-MS	Oxo-, mono-, and di-carboxylic acids	(Kawamura and Gagosian 1987)
GC-MS	Low molecular weight saturated fatty acids	(Mochida et al. 2002)
GC-MS	Low molecular weight fatty acids, fatty alcohols, and sterols	(Fu et al. 2011)
GC-MS; EGA	Saccharides; isoprene products	(Fu et al. 2013)
H-NMR	WIOM; WSOM	(Facchini et al. 2008)
H-NMR	Diethyl and dimethyl amine salts	(Facchini et al. 2010)
H-NMR; LC-MS	Lipids, fatty acids, short chain aliphatics; WSOC	(Decesari et al. 2011)
HPLC	Proteins, amino acids, and polysaccharides in gels	(Kuznetsova et al. 2005)
HPLC	Free amino acids in WSOC	(Matsumoto and Uematsu 2005)
HR-ToF-AMS	Hydrocarbons; oxygenated hydrocarbons	(Ovadnevaite et al. 2011)
HR-ToF-AMS	N/A	(Shank et al. 2012)
IC; EGA	WSOC and TOC	(Yoon et al. 2007)
IC; IC-EIT-MS; EGA	WIOM; levoglucosan, glucose	(Kaku et al. 2006)
IC; solid/liquid phase elemental analysis	WSOC: methanesulfonic acid, alkylammonium salts, dicarboxylic acids	(Rinaldi et al. 2010)
IC; TOC liquid analysis; EGA	WIOC; WSOC aliphatic and partially oxidized humic-like substances	(Cavalli et al. 2004)
IC; TOC liquid analysis; EGA	Enriched in WIOC with high molecular weight; Enriched in WSOC (partly oxidized species with extended aliphatic moieties)	(O'Dowd et al. 2004)

IC; TOC liquid analysis; EGA; Eddy covariance	WIOC; WSOC	(Ceburnis et al. 2008)
IC-EIT-MS	Dicarboxylic acids, carbohydrates	(Crahan et al. 2004)
STXM-NEXAFS	Polysaccharides, proteins, and phytoplankton fragments	(Hawkins and Russell 2010)
TEM	Marine microorganisms; microcolloidal aggregates	(Leck and Bigg 2005)
TEM	WIOC aggregates; exopolymeric gels	(Bigg 2007)
TEM	Exopolymers	(Bigg and Leck 2008)
TOC Analyzer	WSOC, WIOC, TOC	(Sciare et al. 2009)
<b>Generated</b>		
FTIR spectroscopy and HR-ToF-AMS	Polysaccharide-like, alkyl-like, pattern of CH-fragments	(Bates et al. 2012)
H-NMR	WIOM: colloids	(Facchini et al. 2008)
H-NMR	WIOM: lipo-polysaccharides	(Facchini et al. 2010)
Raman microspectroscopy	Aliphatic hydrocarbons	(Ault et al. 2013)
TOC Analyzer	WSOC	(Keene et al. 2007)

<sup>a</sup>Relevant acronyms: Fourier transform ion cyclotron resonance mass spectrometry (FT-ICR MS); Fourier transform infrared (FTIR); gas chromatography mass spectrometry (GC-MS); proton nuclear magnetic resonance (H-NMR); liquid chromatography mass spectrometry (LC-MS); high performance liquid chromatography (HPLC); high resolution time of flight aerosol mass spectrometer (HR-ToF-AMS); ion chromatography (IC); evolved gas analysis (EGA); ion chromatography electrospray ion trap mass spectrometry (IC-EIT-MS); scanning transmission X-ray microscopy with near-edge X-ray absorption fine structure (STXM-NEXAFS); transmission electron microscopy (TEM); total organic carbon (TOC); water insoluble organic mass/carbon (WIOM/C); water soluble organic mass/carbon (WSOM/C).

## Marine Aerosol Measurements during WACS

During the WACS cruise, the R/V *Ronald H. Brown* traveled from Boston, MA, to Bermuda, stopping in the colder, eutrophic seawater of George's Bank and the warmer, oligotrophic seawater of the Sargasso Sea. The nascent (or newly generated) SSA particles, referred to as generated marine aerosol particles, were generated with the Sea Sweep. These particles were free of influence from ambient air and were transported from the sea surface to the research vessel for sampling through a humidity and temperature-controlled inlet.

### FTIR spectroscopy

Ambient and generated marine particles were collected on pre-scanned 37 mm Teflon filters (Pall Inc., 1  $\mu$ m pore size) for 1 to 8 hours, after passing through a diffusion drier filled

with silica gel and a 1  $\mu\text{m}$  cut cyclone. The cyclone has a 100% particle transmission efficiency for particles with aerodynamic diameters ( $d_a$ ) less than 750 nm (Gussman et al. 2002), shown in Figure S1. Five ambient and sixteen generated samples were collected. The filters were analyzed aboard the R/V *Ronald H. Brown* using Fourier transform infrared (FTIR) spectroscopy (Tensor 27 spectrometer, Bruker, Billerica, MA). The filters were then frozen and transported back to San Diego, CA, for further analysis. The generated marine samples were dehydrated using the method outlined by Frossard and Russell (2012) to remove interference of sea salt hydrate bound water with the organic signal in the FTIR spectra.

The FTIR spectrum from each filter was baselined and integrated at specific peak locations to determine the peak areas of the organic functional groups using an automated algorithm outlined by Maria et al. (2002) and revised by Russell et al. (2009) and Takahama et al. (2012). The absorptivity and molar masses were used to convert peak area to mass for each functional group including: organic hydroxyl (C-O-H), alkane (C-C-H), amine (C-N-H), carboxylic acid (COOH), and non-acid carbonyl (C=O). Alkene (C=C-H) and aromatic functional groups were below the detection limit in all of the samples. The total OM for each sample was calculated as the sum of the organic functional groups. 20% uncertainty is shown in Figure 2, based on Maria et al. (2002).

### **HR-ToF-AMS**

A high resolution time of flight aerosol mass spectrometer (HR-ToF-AMS) (Aerodyne, Billerica, MA) was used to measure the non-refractory submicron particle composition of the ambient and generated marine particles including ammonium, sulfate, nitrate, sea salt, and OM concentrations (Canagaratna et al. 2007; DeCarlo et al. 2006). Ambient and generated particles passed through a diffusion drier filled with silica gel and a 1  $\mu\text{m}$  cut cyclone before sampling. The AMS lens has 100% particle transmission efficiency for particles with  $d_a$  from 90 to 700 nm (Figure S1) and 30% transmission efficiency for 1  $\mu\text{m}$  particles ( $d_a$ ) (Williams et al. 2013). The HR-ToF-AMS alternated between sampling in V-mode (both pToF and mass spectrum modes), W-mode, and LS-mode, which is discussed in the next section, on a 2-minute cycle for each mode. The V and W-mode data was analyzed using the ToF-AMS HR Analysis 1.10H program (Pika, D. Sueper, available at <http://cires.colorado.edu/jimenez-group/ToFAMSResources/ToFSoftware/index.html>). However, only V-mode data were used in this study. pCO<sub>2</sub> concentrations were measured during the cruise (Wanninkhof et al. 2013) and used in the ToF-AMS HR analysis program to correct for CO<sub>2</sub> gas phase influence. The ionization efficiency (IE) was obtained using the method described by Jimenez et al. (2003). 20% uncertainty in the HR-ToF-AMS measurements are shown in Figure 2 (Drewnick et al. 2005).

### **LS-ToF-AMS**

A light scattering (LS) module on the HR-ToF-AMS (LS-ToF-AMS) was used to optically detect single particles before characterizing with the mass spectrometer, as described by Liu et al. (2013). The LS-ToF-AMS has the lens efficiency of the HR-ToF-AMS, but the smallest particles with significant optical signal are  $d_a = 180$  nm (Figure S1). Using the LS data processing software Sparrow 1.04D (available at <http://cires.colorado.edu/jimenez-group/ToFAMSResources/ToFSoftware/index.html#Sparrow>), single particles were observed and classified based on their vaporization behavior. Briefly, in order to determine a sufficient chemical signal, ten high intensity ion fragments ( $m/z$  36, 41, 43, 44, 48, 55, 57, 58, 64, 81) were

selected to make up the mass intensity profile for each particle (Liu et al. 2013). Based on the intensity profiles, particles were separated by those that had light scattering and mass spectral signals (LS+MS) and those that only had light scattering signals (LS-only). The LS-only particles were optically detected but not sufficiently vaporized with total mass spectral signal to noise less than 3.

In addition to the optically detected particles, more triggers were saved but did not have detectable optical signals, as described by Liu et al. (2013) as an additional duty cycle due to an unusual noise spike in the LS channel. During sampling, the coincident particles (e.g., more than one particle is optically detected in one cycle) were less than 0.5% of the total particles and are not included in this analysis, consistent with Liu et al. (2013).

### **STXM-NEXAFS**

Ambient and generated particles were collected on silicon nitride windows ( $\text{Si}_3\text{N}_4$ , Silson Ltd, Northampton, England) using a Streaker (PIXE International Corp., Tallahassee, FL) for impaction. The windows were frozen after collection to prevent evaporation. Generated particles were collected from 22:00 to 01:00 UTC starting on 21 August 2012. Ambient particles were collected from 19:00 to 00:00 UTC starting on 23 August 2012. The windows were analyzed at the Advanced Light Source at Lawrence Berkeley National Laboratory using scanning transmission X-ray microscopy with near-edge X-ray absorption fine structure (STXM-NEXAFS) at atmospheric temperature and under dry He at 1 atm (Hawkins and Russell 2010; Takahama et al. 2007; Kilcoyne et al. 2003; Takahama et al. 2010). Scans of selected single particles were done from 278 to 320 eV to determine the X-ray absorption spectra of the carbon K-edge, and functional groups were identified by their absorption (Hawkins and Russell 2010). Image scans of the particles were used to determine the diameter, morphology, and organic composition of the single particles. Due to instrument and analysis constraints, the number of single particles analyzed by STXM-NEXAFS is limited (Bahadur et al. 2010). From the particles impacted on the silicon nitride windows, 26 generated and 18 ambient particles were analyzed.

The generated particle diameters ( $d_p$ ) ranged from 0.65 to 3.1  $\mu\text{m}$ , and the ambient particle diameters ( $d_p$ ) ranged from 0.39 to 2.59  $\mu\text{m}$ . Using a density of 1.1  $\text{g cm}^{-3}$  for the low O/C particles and 2.05  $\text{g cm}^{-3}$  for the high O/C particles (based on a sea salt density of 2.165  $\text{g cm}^{-3}$  and an average sea salt fraction of 89%), the aerodynamic particle diameters ranged from 0.72 to 6.4  $\mu\text{m}$  and 0.47 to 5.3  $\mu\text{m}$  for generated and ambient marine particles, respectively (Figure S1).

### **OC and IC measurements**

Ambient and generated particles (<1.1  $\mu\text{m}$  at 60% relative humidity) were collected on pre-combusted quartz fiber filters using a two stage impactor downstream of a charcoal denuder (Bates et al. 2004). They were analyzed with a Sunset Laboratory thermal/optical analyzer to determine the concentrations of organic carbon (OC) with evolved gas analysis, hereafter referred to as EGA OC. Particles (<1.1  $\mu\text{m}$ ) were also collected on Millipore Fluoropore filters with a Berner-type multijet cascade impactor. The substrates were extracted and analyzed using ion chromatography (IC) to quantify inorganic ions including  $\text{Na}^+$ ,  $\text{Cl}^-$ , sulfate, nitrate, and ammonium (Quinn et al. 1998).

Sea salt concentrations for the generated marine particles were calculated as  $3.26 \cdot \text{Na}^+$  concentrations measured by IC, based on the calculation by Quinn et al. (submitted) and the ratio of ions in seawater (Holland 1978). Ambient sea salt concentrations were calculated using measured  $\text{Cl}^-$  plus  $1.47 \cdot \text{Na}^+$  concentrations to account for the depletion of  $\text{Cl}^-$  in the atmosphere (Holland 1978). As described by Quinn et al. (in review) using these measurements, the generated marine particle mass was 89% sea salt and 11% OM. The ambient particle mass was 3% sea salt, 59% OM, and 38% other mass (Table S2).

Table S2: Mass fractions of OM, non-sea salt sulfate, ammonium, methanesulfonic acid (MSA), and sea salt in ambient and generated marine particles (based on Quinn et al., (in review)).

	<b>Ambient</b>	<b>Generated</b>
OM (FTIR)	0.59	0.11
Non-sea salt sulfate	0.25	
Ammonium	0.11	
MSA	0.02	
Sea salt	0.03	0.89

### **Aerosol physical measurements**

Ambient and generated marine aerosol size distributions were measured using differential mobility particle sizers (DMPS, Aitken and Accumulation) and an aerodynamic particle sizer (APS, TSI model 3321) as described by Bates et al. (2012). The number and mass size distributions for the generated and ambient marine particles are shown in Figure S1.

The 100% transmission efficiency aerodynamic diameter ( $d_a$ ) ranges for FTIR spectroscopy, HR-ToF-AMS, and LS-ToF-AMS, in addition to the range of particles analyzed by STXM-NEXAFS, are included in Figure S1 and listed in Table 1. Figure S1 shows the overlap of the  $d_a$  ranges with the maximum concentration ranges for the LS-ToF-AMS, HR-ToF-AMS, and FTIR measurements. The STXM-NEXAFS technique measured particles with larger  $d_a$  but overlaps with the other techniques at their largest  $d_a$  values.

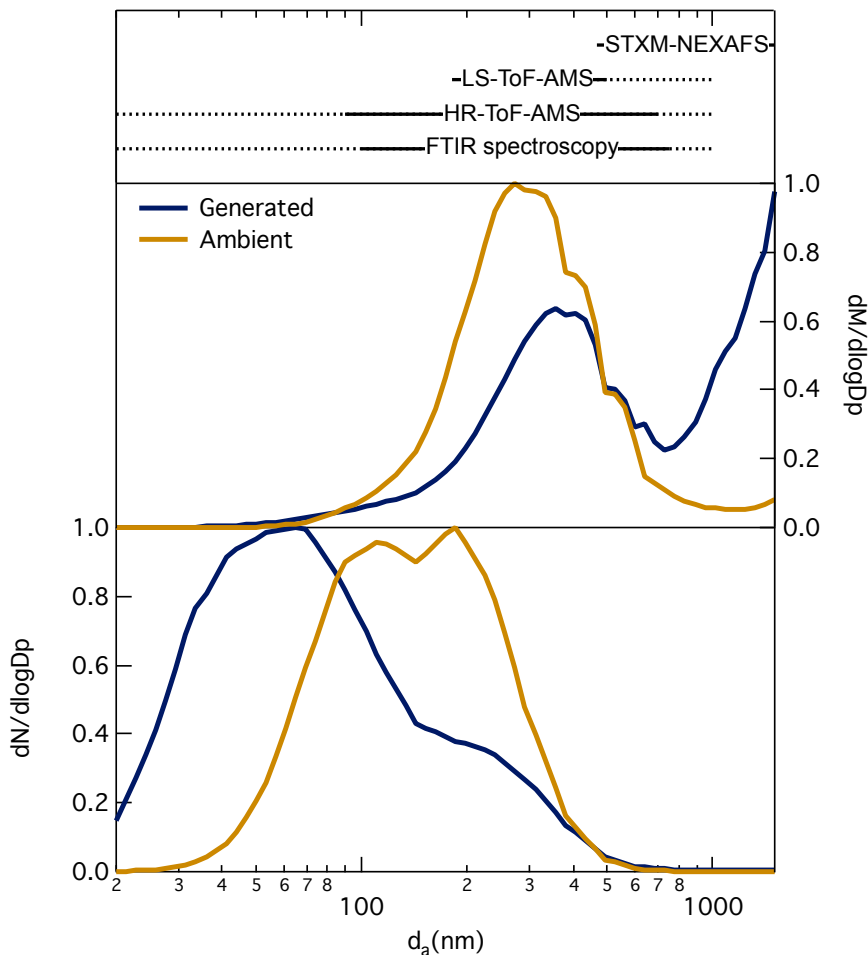


Figure S1: Normalized (bottom) number and (middle) mass size distributions of generated and ambient marine aerosol particles. (top) Ranges of aerodynamic diameters of particles measured with the different techniques, based on Table 1. The solid lines represent 100% particle transmission efficiency for HR-ToF-AMS and FTIR, the lowest detectable diameters to diameters with 100% transmission efficiency for LS-ToF-AMS, and the diameters of particles measured for STXM-NEXAFS. Dashed lines show the reduced collection on filters and reduced sensitivity for FTIR and 50% transmission efficiency for HR-ToF-AMS and LS-ToF-AMS. At 1  $\mu\text{m}$ , the HR-ToF-AMS and LS-ToF-AMS have particle transmission efficiencies of 30%.”

### Comparison of HR-ToF-AMS and FTIR OC with EGA OC

The OC mass measured by FTIR spectroscopy was calculated from the total moles of carbon in each sample. On average, the total OC mass measured by FTIR spectroscopy was a factor of 1.06 greater than that measured with the Sunset EGA ( $r = 0.61$ ) with an average overall percent difference of 3% (Figure S2a). HR-ToF-AMS OC was calculated using the ratio of OM/OC and OM. Overall, comparison with EGA OC gave a slope of 0.31 and a correlation of  $r = 0.67$  (Figure S2b). The HR-ToF-AMS and FTIR OM have similar masses after the  $CE_{IC}$  is applied (Figure S2c), and the ambient samples correlate well ( $r = 0.88$ ).

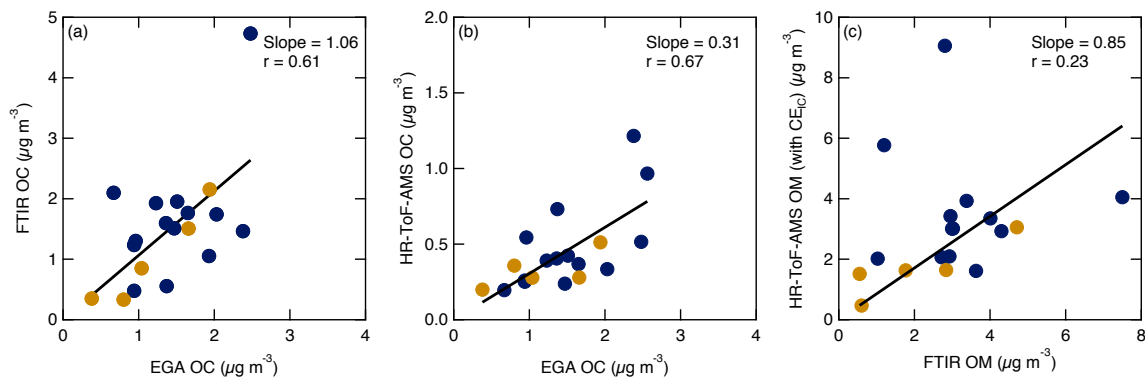


Figure S2: Correlations of (a) FTIR OC with EGA OC; (b) HR-ToF-AMS OC with EGA OC; and (c) HR-ToF-AMS OM (using  $CE_{IC}$ ) with FTIR OM. Markers are colored as generated (dark blue) and ambient (bronze). The overall (ambient and generated together) slopes and correlations are given. Two samples were not included in the correlations due to filter sampling problems and high humidity.

Table S3: Ambient and generated marine particle OM, OC, and O/C values measured with FTIR spectroscopy, HR-ToF-AMS, and EGA (OC only). HR-ToF-AMS OC was calculated with HR-ToF-AMS OM/OC elemental ratios. HR-ToF-AMS values do not have a CE applied.

	Ambient	Generated
<b>OM (<math>\mu\text{g m}^{-3}</math>)</b>		
FTIR	$2.09 \pm 1.74$	$3.23 \pm 1.52$
HR-ToF-AMS	$0.58 \pm 0.32$	$0.65 \pm 0.36$
<b>OC (<math>\mu\text{g m}^{-3}</math>)</b>		
EGA	$1.16 \pm 0.63$	$1.68 \pm 0.75$
FTIR	$1.04 \pm 0.79$	$1.67 \pm 1.01$
HR-ToF-AMS	$0.33 \pm 0.12$	$0.49 \pm 0.30$
<b>O/C</b>		
FTIR	$0.55 \pm 0.17$	$0.51 \pm 0.22$
HR-ToF-AMS	$0.63 \pm 0.11$	$0.20 \pm 0.08$

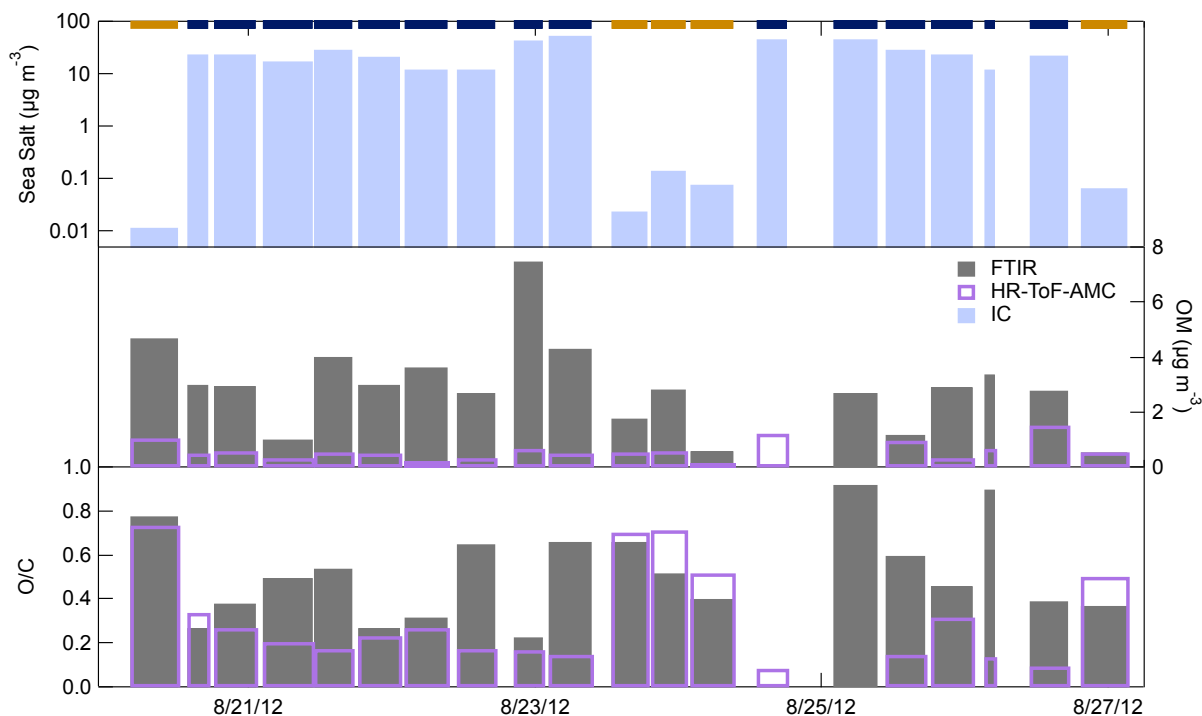


Figure S3: Time series of (top) IC sea salt concentration, (middle) FTIR spectroscopy and HR-ToF-AMS (no CE applied) OM concentrations, and (bottom) FTIR and HR-ToF-AMS O/C ratios. The bars at the top represent the type of sample: ambient (bronze) and generated (dark blue) marine aerosol.

### HR-ToF-AMS Sea Salt

The heater temperature of the HR-ToF-AMS was set to 650°C to vaporize more of the sea salt components (Ovadnevaite et al. 2012). The HR-ToF-AMS measurements were used to calculate the mass of sea salt by identifying and scaling specific sea salt ions based on the method outlined by Ovadnevaite et al. (2012). The concentrations of four different combinations of the sea salt ions, outlined in Table S4, were averaged over the impactor sampling times. A least squares fit was used to fit the concentrations from the ion groups in Table S4 to the IC measured sea salt to determine a HR-ToF-AMS sea salt scaling factor, which is the inverse of the sea salt collection efficiency ( $CE_{SS}$ ). The combination of sea salt ions  $Cl^+$ ,  $HCl^+$ ,  $NaCl^+$ ,  $Na_2Cl^+$ ,  $KCl^+$ ,  $MgCl^+$  and their isotopes were used to calculate the final scaling factor based on the correlation to IC sea salt and the combined ion signal. The ambient scaling factor is 12, and the generated marine particle scaling factor is 79, which are similar to those used by Ovadnevaite et al. (2012) of 2.5 and 51, respectively, calculated for laboratory generated sea salt. The larger sea salt scaling factors measured here may be due to a decreased lens transmission efficiency of larger sea salt particles, compared to the monodisperse 300 nm particles used by Ovadnevaite et al. (2012). Increasing the number of HR-ToF-AMS sea salt ions in the comparison to IC sea salt decreases the resulting scaling factor. While  $NaCl^+$  compared well to the IC sea salt ( $r > 0.70$ ), the scaling factor was very high for both ambient (1302) and generated (1729) marine particles making the corresponding  $CE_{SS}$  values very low and indicating that additional ions are needed for the scaling. The concentration of  $Na^+$  is unreliable as a sea salt ion due to its persistence in

the HR-ToF-AMS system and was therefore not used to calculate the scaling factor (Ovadnevaite et al. 2012). The moderate correlations of the HR-ToF-AMS ions and the IC sea salt suggest that the sea salt collection efficiency may also have a size dependence. A more accurate CE could be determined using variations in size and lens transmission efficiency.

Table S4: Comparison of sea salt scaling factors ( $1/CE_{SS}$ ) used to scale HR-ToF-AMS sea salt to IC measured sea salt. The correlation coefficient is shown in parentheses for each case. The average of un-scaled and scaled sea salt is shown for each set of ions.

		Scaling factor (correlation coefficient, r)		Average of HR-ToF-AMS sea salt ( $\mu\text{g m}^{-3}$ )			
		Ambient	Generated	Un-scaled		Scaled <sup>b</sup>	
HR-ToF-AMS ions used to calculate sea salt	Reference Values			Ambient	Generated	Ambient	Generated
NaCl <sup>+</sup>	51 <sup>a</sup>	1302 (0.98)	1729 (0.71)	9.5e-5	0.015	0.12	25.2
Na <sup>+</sup> , Cl <sup>+</sup> , HCl <sup>+</sup> , NaCl <sup>+</sup> , <sup>37</sup> Cl <sup>+</sup> , H <sup>37</sup> Cl <sup>+</sup> , Na <sup>37</sup> Cl <sup>+</sup>	2.5 <sup>a</sup>	0.216 (0.65)	27 (0.55)	0.43	1.0	0.09	28.2
NaCl <sup>+</sup> , Na <sub>2</sub> Cl, KCl <sup>+</sup> , MgCl <sup>+</sup> , Na <sup>37</sup> Cl <sup>+</sup> , Na <sub>2</sub> <sup>37</sup> Cl K <sup>37</sup> Cl <sup>+</sup> , <sup>41</sup> KCl <sup>+</sup> , <sup>41</sup> K <sup>37</sup> Cl <sup>+</sup> , Mg <sup>37</sup> Cl <sup>+</sup>	N/A	126 (0.20)	707 (0.67)	9.1e-4	0.037	0.12	25.8
Cl <sup>+</sup> , HCl <sup>+</sup> , NaCl <sup>+</sup> , Na <sub>2</sub> Cl <sup>+</sup> , KCl <sup>+</sup> , MgCl <sup>+</sup> , <sup>37</sup> Cl <sup>+</sup> , H <sup>37</sup> Cl <sup>+</sup> , Na <sup>37</sup> Cl <sup>+</sup> , Na <sub>2</sub> <sup>37</sup> Cl <sup>+</sup> , K <sup>37</sup> Cl <sup>+</sup> , <sup>41</sup> KCl <sup>+</sup> , <sup>41</sup> K <sup>37</sup> Cl <sup>+</sup> , Mg <sup>37</sup> Cl <sup>+</sup>	N/A	12 (0.52)	79 (0.59)	9.9e-3	0.35	0.12	27.6

<sup>a</sup>(Ovadnevaite et al. 2012); laboratory generated sea salt (300 nm, relative humidity = 65%) and vaporizer temperature of 650°C

<sup>b</sup>Average IC sea salt values: ambient = 0.10  $\mu\text{g m}^{-3}$  and generated = 26.7  $\mu\text{g m}^{-3}$

## HR-ToF-AMS CE Calculations

The HR-ToF-AMS collection efficiency (CE) was calculated by comparing the concentration of HR-ToF-AMS sulfate and the concentration of sulfate from filters measured with IC, as discussed by Canagaratna et al. (2007) and calculated by Bates et al. (2012) for similar measurements. The sulfate based CE ( $CE_{IC}$ ) was calculated separately for the ambient and generated marine particles to allow for the differences in CE values based on particle type. With the direct comparison to independently measured sulfate, other factors contributing to the CE, such as particle shape, phase, and acidity are taken in to account but not directly calculated (Matthew et al. 2008; Huffman et al. 2005; Middlebrook et al. 2012). This method also includes lens transmission efficiency, which affects the larger particles, such as the OM associated with sea salt. When comparing the HR-ToF-AMS sulfate loadings to IC sulfate only, we obtained a  $CE_{IC}$  of 0.35 for ambient, and a  $CE_{IC}$  of 0.17 for the generated particles. The different  $CE_{IC}$

values for ambient and generated marine particles indicate that the  $CE_{IC}$  incorporates variations in detection efficiency as a function of particle size. The  $CE_{IC}$  values were used to scale the OM for comparison with FTIR measured OM.

The  $CE_{IC}$  values for generated particles are less than typical AMS CE values of 0.5 (Canagaratna et al. 2007) because a large fraction of the generated particle mass (89%) is sea salt, which does not vaporize efficiently at 650°C (due to its refractory nature and tendency to bounce off the vaporizer) and therefore has a much lower CE ( $CE_{SS}$ ). For this reason, and to compare directly to LS-ToF-AMS that produces a total CE for all particles through optical detection, a total CE ( $CE_{total}$ ) for the HR-ToF-AMS was calculated separately for the ambient ( $CE_{totalA}$ ) and generated ( $CE_{totalG}$ ) particles using:  $CE_{total} = CE_{SS} * X_{SS} + CE_{other} * X_{other}$ . The value of  $CE_{other}$  is assumed to be 0.5 (Canagaratna et al. 2007), and X is the fraction of the respective mass measured by IC and/or EGA. The calculated  $CE_{totalG}$  (0.07) is less than  $CE_{totalA}$  (0.49), indicating that only a small fraction of the total mass is vaporized by the HR-ToF-AMS under the standard operational conditions due to the presence of sea salt. The standard comparison of total particle mass to integrated particle mass size distributions was not included due to differences in sampling conditions between the HR-ToF-AMS and the particle sizing instruments.

### **STXM-NEXAFS Particle Morphologies**

The particle morphologies associated with these spectral types were unique to the OM types. The low O/C particle type mainly had round or irregular shaped particles with uniformly distributed carbon absorbance. A large fraction of the high O/C particles have the shapes characteristic of polysaccharides on sea salt, with a cuboidal inner-structure surrounded by a high O/C organic (Hawkins and Russell 2010; Russell et al. 2010). Four of the 17 ambient high O/C particles were round and did not have characteristics of organics on sea salt. These particles may be from oxidization of alkyl-like particles or secondary formation in the atmosphere. Their spectra are similar to secondary organic aerosol particles identified by Takahama et al. (2007). STXM-NEXAFS measurements are too limited (in size range and sample number) to be quantitatively representative of the OM particle.

### **LS-ToF-AMS and HR-ToF-AMS**

The composition of the LS-ToF-AMS particles has a much larger fraction of low O/C OM than the HR-ToF-AMS for both the generated and ambient marine particles. This difference may be attributed to a number of factors. (i) The high and low O/C separation for the LS-ToF-AMS was based on a single particle clustering, where the HR-ToF-AMS OM separation was based on the mass fragment groups of the overall average mass spectra. (ii) Additionally, spectra with less than 6 organic ions were not used in the LS-ToF-AMS clustering as their composition was not representative of the particle. However, those spectra are included in the overall HR-ToF-AMS OM due to the overall mass averaging during sampling. The same idea applies to the spectra that were saved by the light scattering mode. If a significant mass spectrum was not observed, then that spectrum was not used. For the HR-ToF-AMS, all of the mass spectra are averaged, so the lack of ions in an individual spectrum does not affect the total. The low OM signal from the generated particles is better included in the bulk averaged HR-ToF-AMS than in the individual particles detected by LS-ToF-AMS. (iii) The LS-ToF-AMS has a smaller range of

measured particles than the HR-ToF-AMS. The smallest particle with significant optically detected signal is 180 nm ( $d_a$ ). This is a higher cutoff than the HR-ToF-AMS, which has a particle transmission efficiency of 100% at 90 nm ( $d_a$ ). The LS-ToF-AMS particle size detection range falls within the size range of the maximum in particle mass concentration but does not have much overlap with the maximum in number concentration for the generated marine particles. (iv) Particles that contain less volatile species, such as sea salt, can bounce off of the vaporizer (Huffman et al. 2005).

## References

- Ault, A. P., D. F. Zhao, C. J. Ebben, M. J. Tauber, F. M. Geiger, K. A. Prather, and V. H. Grassian (2013), Raman microspectroscopy and vibrational sum frequency generation spectroscopy as probes of the bulk and surface compositions of size-resolved sea spray particles, *Physical Chemistry - Chemical Physics*, 15(17), 6206-6214, doi: 10.1039/c3cp43899f
- Bahadur, R., L. M. Russell, and K. Prather (2010), Composition and Morphology of Individual Combustion, Biomass Burning, and Secondary Organic Particle Types Obtained Using Urban and Coastal ATOFMS and STXM-NEXAFS Measurements, *Aerosol Science and Technology*, 44(7), 551-562, doi:10.1080/02786821003786048.
- Bates, T. S., et al. (2004), Marine boundary layer dust and pollutant transport associated with the passage of a frontal system over eastern Asia, *Journal of Geophysical Research*, 109(D19), 18 pp., doi:10.1029/2003jd004094.
- Bates, T. S., et al. (2012), Measurements of Ocean Derived Aerosol off the Coast of California, *Journal of Geophysical Research - Atmospheres*, 117(D00V15), doi:10.1029/2012JD017588.
- Bigg, E. K. (2007), Sources, nature and influence on climate of marine airborne particles, *Environmental Chemistry*, 4(3), 155-161, doi:10.1071/en07001.
- Bigg, E. K., and C. Leck (2008), The composition of fragments of bubbles bursting at the ocean surface, *Journal of Geophysical Research-Atmospheres*, 113(D11), doi:10.1029/2007jd009078.
- Canagaratna, M. R., et al. (2007), Chemical and microphysical characterization of ambient aerosols with the aerodyne aerosol mass spectrometer, *Mass Spectrometry Reviews*, 26(2), 185-222, doi:10.1002/mas.20115.
- Cavalli, F., et al. (2004), Advances in characterization of size-resolved organic matter in marine aerosol over the North Atlantic, *Journal of Geophysical Research-Atmospheres*, 109(D24215), doi:10.1029/2004jd005137.
- Ceburnis, D., C. D. O'Dowd, G. S. Jennings, M. C. Facchini, L. Emblico, S. Decesari, S. Fuzzi, and J. Sakalys (2008), Marine aerosol chemistry gradients: Elucidating primary and secondary processes and fluxes, *Geophysical Research Letters*, 35(7), doi:10.1029/2008gl033462.
- Crahan, K. K., D. A. Hegg, D. S. Covert, H. Jonsson, J. S. Reid, D. Khelif, and B. J. Brooks (2004), Speciation of organic aerosols in the tropical mid-pacific and their relationship to light scattering, *Journal of the Atmospheric Sciences*, 61(21), 2544-2558, doi: 10.1175/JAS3284.1
- DeCarlo, P. F., et al. (2006), Field-deployable, high-resolution, time-of-flight aerosol mass spectrometer, *Analytical Chemistry*, 78(24), 8281-8289, doi:10.1021/ac061249n.
- Decesari, S., Finessi, E., Rinaldi, M., Paglione, M., Fuzzi, S., Stephanou, E. G., Tzias, T., Spyros, A., Ceburnis, D., O'Dowd, C., Dall'Osto, M., Harrison, R. M., Allan, J., Coe, H. and Facchini, M. C. (2011), Primary and secondary marine organic aerosols over the North Atlantic Ocean during the MAP experiment, *Journal of Geophysical Research-Atmospheres*, 116, 21, doi:10.1029/2011jd016204.
- Drewnick, F., et al. (2005), A new time-of-flight aerosol mass spectrometer (TOF-AMS) - Instrument description and first field deployment, *Aerosol Science and Technology*, 39(7), 637-658, doi: 10.1080/02786820500182040.

- Facchini, M. C., et al. (2008), Primary submicron marine aerosol dominated by insoluble organic colloids and aggregates, *Geophysical Research Letters*, L17814 (17815 pp.), doi:10.1029/2008gl034210.
- Facchini, M. C., M. Rinaldi, S. Decesari, and S. Fuzzi (2010), Marine organic aerosol and biological oceanic activity, *Chemical Engineering*, 22, 107-112, doi: 10.3303/CET1022017.
- Frossard, A. A., and L. M. Russell (2012), Removal of Sea Salt Hydrate Water from Seawater-Derived Samples by Dehydration, *Environmental Science & Technology*, 46(24), 13326-13333, doi:10.1021/es3032083.
- Fu, P. Q., K. Kawamura, J. Chen, B. Charriere, and R. Sempere (2013), Organic molecular composition of marine aerosols over the Arctic Ocean in summer: contributions of primary emission and secondary aerosol formation, *Biogeosciences*, 10(2), 653-667, doi:10.5194/bg-10-653-2013.
- Fu, P. Q., K. Kawamura, and K. Miura (2011), Molecular characterization of marine organic aerosols collected during a round-the-world cruise, *Journal of Geophysical Research-Atmospheres*, 116, doi:10.1029/2011jd015604.
- Gussman, R. A., L. C. Kenny, M. Labickas, and P. Norton (2002), Design, calibration, and field test of a cyclone for PM1 ambient air sampling, *Aerosol Science and Technology*, 36(3), 361-365, doi:10.1080/027868202753504461.
- Hawkins, L. N., and L. M. Russell (2010), Polysaccharides, Proteins, and Phytoplankton Fragments: Four Chemically Distinct Types of Marine Primary Organic Aerosol Classified by Single Particle Spectromicroscopy, *Advances in Meteorology*, 2010(Article ID 612132), 14, doi:10.1155/2010/612132.
- Holland, H. D. (1978), *The Chemistry of the Atmosphere and Oceans*, edited, p. 154, Jon Wiley, New York.
- Huffman, J. A., J. T. Jayne, F. Drewnick, A. C. Aiken, T. Onasch, D. R. Worsnop, and J. L. Jimenez (2005), Design, modeling, optimization, and experimental tests of a particle beam width probe for the aerodyne aerosol mass spectrometer, *Aerosol Science and Technology*, 39(12), 1143-1163, doi:10.1080/02786820500423782.
- Jimenez, J. L., et al. (2003), Ambient aerosol sampling using the Aerodyne Aerosol Mass Spectrometer, *Journal of Geophysical Research-Atmospheres*, 108(D7), doi:10.1029/2001jd001213.
- Kaku, K. C., D. A. Hegg, D. S. Covert, J. L. Santarpià, H. Jonsson, G. Buzorius, and D. R. Collins (2006), Organics in the Northeastern Pacific and their impacts on aerosol hygroscopicity in the subsaturated and supersaturated regimes, *Atmospheric Chemistry and Physics*, 6, 4101-4115.
- Kawamura, K., and R. B. Gagosian (1987), Implications of omega-oxocarboxylic acids in the remote marine atmosphere for photooxidation of unsaturated fatty-acids, *Nature*, 325(6102), 330-332, doi:10.1038/325330a0.
- Keene, W. C., et al. (2007), Chemical and physical characteristics of nascent aerosols produced by bursting bubbles at a model air-sea interface, *Journal of Geophysical Research-Atmospheres*, 112(D21), doi:10.1029/2007jd008464.
- Kilcoyne, A. L. D., et al. (2003), Interferometer-controlled scanning transmission X-ray microscopes at the Advanced Light Source, *Journal of Synchrotron Radiation*, 10, 125.
- Kuznetsova, M., C. Lee, and J. Aller (2005), Characterization of the proteinaceous matter in marine aerosols, *Marine Chemistry*, 96(3-4), 359-377, doi:10.1016/j.marchem.2005.03.007.

- Leck, C., and E. K. Bigg (2005), Source and evolution of the marine aerosol - A new perspective, *Geophysical Research Letters*, 32(L19803), doi:10.1029/2005gl023651.
- Liu, S., L. M. Russell, D. T. Sueper, and T. B. Onasch (2013), Organic particle types by single-particle measurements using a time-of-flight aerosol mass spectrometer coupled with a light scattering module, *Atmospheric Measurement Techniques*, 6(2), 187-197, doi:10.5194/amt-6-187-2013.
- Maria, S. F., L. M. Russell, B. J. Turpin, and R. J. Poreja (2002), FTIR measurements of functional groups and organic mass in aerosol samples over the Caribbean, *Atmospheric Environment*, 36(33), 5185-5196.
- Matsumoto, K., and M. Uematsu (2005), Free amino acids in marine aerosols over the western North Pacific Ocean, *Atmospheric Environment*, 39(11), 2163-2170, doi:10.1016/j.atmosenv.2004.12.022.
- Matthew, B. M., A. M. Middlebrook, and T. B. Onasch (2008), Collection efficiencies in an Aerodyne Aerosol Mass Spectrometer as a function of particle phase for laboratory generated aerosols, *Aerosol Science and Technology*, 42(11), 884-898, doi:10.1080/02786820802356797.
- Middlebrook, A. M., R. Bahreini, J. L. Jimenez, and M. R. Canagaratna (2012), Evaluation of Composition-Dependent Collection Efficiencies for the Aerodyne Aerosol Mass Spectrometer using Field Data, *Aerosol Science and Technology*, 46(3), doi:10.1080/02786826.2011.620041.
- Mochida, M., Y. Kitamori, K. Kawamura, Y. Nojiri, and K. Suzuki (2002), Fatty acids in the marine atmosphere: Factors governing their concentrations and evaluation of organic films on sea-salt particles, *Journal of Geophysical Research-Atmospheres*, 107(D17), 10.1029/2001JD001278.
- O'Dowd, C. D., M. C. Facchini, F. Cavalli, D. Ceburnis, M. Mircea, S. Decesari, S. Fuzzi, Y. J. Yoon, and J. P. Putaud (2004), Biogenically driven organic contribution to marine aerosol, *Nature*, 431(7009), 676-680, doi:10.1038/nature02959.
- Ovadnevaite, J., D. Ceburnis, M. Canagaratna, H. Berresheim, J. Bialek, G. Martucci, D. R. Worsnop, and C. O'Dowd (2012), On the effect of wind speed on submicron sea salt mass concentrations and source fluxes, *Journal of Geophysical Research-Atmospheres*, 117, doi:10.1029/2011jd017379.
- Ovadnevaite, J., C. O'Dowd, M. Dall'Osto, D. Ceburnis, D. R. Worsnop, and H. Berresheim (2011), Detecting high contributions of primary organic matter to marine aerosol: A case study, *Geophysical Research Letters*, 38, doi:10.1029/2010gl046083.
- Quinn, P. K., T. S. Bates, K. S. Schultz, D. C. Coffman, A. A. Frossard, L. M. Russell, W. C. Keene, and D. J. Kieber (in review), Empirical Constraints on Modeling the Organic Matter Enrichment in Nascent Sea Spray Aerosol, *Nature Geoscience*.
- Quinn, P. K., D. J. Coffman, V. N. Kapustin, T. S. Bates, and D. S. Covert (1998), Aerosol optical properties in the marine boundary layer during the First Aerosol Characterization Experiment (ACE 1) and the underlying chemical and physical aerosol properties, *Journal of Geophysical Research-Atmospheres*, 103(D13), 16547-16563.
- Rinaldi, M., S. Decesari, E. Finessi, L. Giulianelli, C. Carbone, S. Fuzzi, C. D. O'Dowd, D. Ceburnis, and M. C. Facchini (2010), Primary and secondary organic marine aerosol and oceanic biological activity: recent results and new perspectives for future studies, *Advances in Meteorology*, 2010(Arctic ID 310682), 10, doi: 10.1155/2010/310682.

- Russell, L. M., L. N. Hawkins, A. A. Frossard, P. K. Quinn, and T. S. Bates (2010), Carbohydrate-like composition of submicron atmospheric particles and their production from ocean bubble bursting, *Proceedings of the National Academy of Sciences of the United States of America*, 107(15), 6652-6657, doi:10.1073/pnas.0908905107.
- Russell, L. M., S. Takahama, S. Liu, L. N. Hawkins, D. S. Covert, P. K. Quinn, and T. S. Bates (2009), Oxygenated fraction and mass of organic aerosol from direct emission and atmospheric processing measured on the R/V Ronald Brown during TEXAQS/GoMACCS 2006, *Journal of Geophysical Research-Atmospheres*, 114, doi:10.1029/2008jd011275.
- Schmitt-Kopplin, P., et al. (2012), Dissolved organic matter in sea spray: a transfer study from marine surface water to aerosols, *Biogeosciences*, 9(4), doi:10.5194/bg-9-1571-2012.
- Sciare, J., O. Favez, R. Sarda-Estève, K. Oikonomou, H. Cachier, and V. Kazan (2009), Long-term observations of carbonaceous aerosols in the Austral Ocean atmosphere: Evidence of a biogenic marine organic source, *Journal of Geophysical Research-Atmospheres*, 114, doi:10.1029/2009jd011998.
- Shank, L. M., S. Howell, A. D. Clarke, S. Freitag, V. Brekhovskikh, V. Kapustin, C. McNaughton, T. Campos, and R. Wood (2012), Organic matter and non-refractory aerosol over the remote Southeast Pacific: oceanic and combustion sources, *Atmospheric Chemistry and Physics*, 12(1), doi:10.5194/acp-12-557-2012.
- Takahama, S., S. Gilardoni, L. M. Russell, and A. L. D. Kilcoyne (2007), Classification of multiple types of organic carbon composition in atmospheric particles by scanning transmission X-ray microscopy analysis, *Atmospheric Environment*, 41(40), 9435-9451, doi:10.1016/j.atmosenv.2007.08.051.
- Takahama, S., A. Johnson, and L. M. Russell (2012), Quantification of carboxylic and carbonyl functional groups in organic aerosol infrared absorbance spectra, *Aerosol Science and Technology*, doi:10.1080/02786826.2012.752065.
- Takahama, S., S. Liu, and L. M. Russell (2010), Coatings and clusters of carboxylic acids in carbon-containing atmospheric particles from spectromicroscopy and their implications for cloud-nucleating and optical properties, *Journal of Geophysical Research-Atmospheres*, 115, 21, doi:10.1029/2009jd012622.
- Wanninkhof, R., R. D. Castle, and J. Shannahoff (2013), Underway pCO<sub>2</sub> measurements aboard the R/V Ronald H. Brown during the 2012 cruises, [http://cdiac.ornl.gov/ftp/oceans/VOS\\_Ronal\\_Brown/RB2012/](http://cdiac.ornl.gov/ftp/oceans/VOS_Ronal_Brown/RB2012/). Carbon Dioxide Information Analysis Center, Oak Ridge National Laboratory, US Department of Energy, Oak Ridge, Tennessee, doi:10.3334/CDIAC/OTG.VOS\_RB\_2012.
- Williams, L. R., et al. (2013), Characterization of an aerodynamic lens for transmitting particles greater than 1 micrometer in diameter into the Aerodyne aerosol mass spectrometer, *Atmospheric Measurement Techniques*, 6, 3271-3280, doi:10.5194/amt-6-3271-2013.
- Yoon, Y. J., et al. (2007), Seasonal characteristics of the physicochemical properties of North Atlantic marine atmospheric aerosols, *Journal of Geophysical Research-Atmospheres*, 112(D04206), doi: 10.1029/2005jd007044.